J|A|C|S
ARTICLES
Published on Web 01/21/2006

Structural Insights into Homo- and Heterotropic Allosteric Coupling in the Zinc Sensor *S. aureus* CzrA from Covalently Fused Dimers

Sunbae Lee, Alphonse I. Arunkumar, Xiaohua Chen, and David P. Giedroc*

Contribution from the Department of Biochemistry and Biophysics, Texas A&M University, College Station, Texas 77843-2128

Received July 13, 2005; E-mail: giedroc@tamu.edu

Abstract: The Zn(II)/Co(II)-sensing transcriptional repressor, *Staphylococcus aureus* CzrA, is a homodimer containing a symmetry-related pair of subunit-bridging tetrahedral N_3O metal sensor coordination sites. A metal-induced quaternary structural change within the homodimer is thought to govern the biological activity of this and other metal sensor proteins. Here, we exploit covalent $(Gly_4Ser)_n$ linkers of variable length in "fused" CzrAs, where $n = 1$ (designated 5L-fCzrA), 2 (10L-fCzrA), or 3 (15L-fCzrA), as molecular rulers designed to restrict any quaternary structural changes that are associated with metal binding and metal-mediated allosteric regulation of DNA binding to varying degrees. While 15L-fCzrA exhibits properties most like homodimeric CzrA, shortening the linker in 10L-fCzrA abolishes negative homotropic cooperativity of Zn(II) binding and reduces DNA binding affinity of the apoprotein significantly. Decreasing the linker length further in 5L-fCzrA effectively destroys one metal site altogether and further reduces DNA binding affinity. However, Zn(II) negatively regulates DNA binding of all fCzrAs, with allosteric coupling free energies (ΔG^1_c) of 4.6, 3.1, and 2.7 kcal mol^{-1} for 15L-, 10L-, and 5L-fCzrAs, respectively. Introduction of a single nonliganding H97N substitution into either the N-terminal or C-terminal protomer domain in 10L-fCzrA results in $\Delta G^1_c = 2.6$ kcal mol^{-1} or ≈83% that of 10L-fCzrA; in contrast, homodimeric H97N CzrA gives $\Delta G^1_c = 0$. $^1H-^{15}N$ HSQC spectra acquired for *wt*-, 10L-fCzrA and H97N 10L-fCzrA in various Zn(II) ligation states reveal that the allosteric change of the protomer domains within the fused dimer is independent and not concerted. Thus, occupancy of a single metal site by Zn(II) introduces asymmetry into the CzrA homodimer that leads to significant allosteric regulation of DNA binding.

Introduction

Although metal ions are indispensable in various cellular processes including protein folding, enzymatic catalysis, and signal transduction, at high concentrations they become extremely toxic.[1] All cells must be capable of "sensing" intracellular concentrations of metal ions, to appropriately induce the expression of genes encoding specific metal uptake or efflux/sequestration proteins to effect homeostasis of essential metal ions.[2] Overlapping or similar regulatory mechanisms have evolved to sense toxic metal pollutants, e.g., cadmium, mercury, arsenic, and lead, that play no beneficial biological role.[3] The ArsR/SmtB[4] and MerR[5] families of winged helix−loop−helix proteins control the expression of genes that mediate metal ion detoxification and resistance in prokaryotes under conditions of metal ion excess, and members of each family have been identified that have evolved to sense both biologically required transition metal ions and toxic metal pollutants.

Staphylococcus aureus CzrA is a well-characterized Zn(II)/Co(II)-responsive transcriptional repressor from the ArsR/SmtB family which regulates transcription of the *czr* operon in response to Zn(II) and Co(II) in vivo;[6,7] a CzrA homologue has recently been discovered in *B. subtilus*.[8] The *czr* operon encodes CzrB, a metal transporter from the cation diffusion facilitator (CDF) family homologous to *E. coli* ZitB.[9] Expression of the *czr* operon is transcriptionally induced by high concentrations of Zn(II) or Co(II) only. CzrA is a homodimeric protein from the winged-helix family ($\alpha\alpha\alpha\alpha\beta\beta\alpha$) and harbors two metal binding sites at the dimer interface.[10] Zn(II) ions are bound to a pair of tetrahedral, interhelical binding sites, with two ligands derived from the α5 helix of one subunit, D84 $O^{\delta1}$, H86 $N^{\delta1}$, and two from the α5 helix of the other subunit, H97′ $N^{\delta1}$ and H100′ $N^{\epsilon2}$.[11] Crystallographic studies on the related zinc sensor from the cyanobacterium *Synechococcus*, SmtB, reveals that

(1) Finney, L. A.; O'Halloran, T. V. *Science* **2003**, *300*, 931−936.
(2) Nies, D. H.; Brown, N. L. *Metal Ions in Gene Regulation*; Chapman & Hall: New York, 1998; pp 77−103.
(3) Pennella, M. A.; Giedroc, D. P. *Biometals* **2005**, *18*, 413−428.
(4) Busenlehner, L. S.; Pennella, M. A.; Giedroc, D. P. *FEMS Microbiol. Rev.* **2003**, *27*, 131−143.
(5) Brown, N. L.; Stoyanov, J. V.; Kidd, S. P.; Hobman, J. L. *FEMS Microbiol. Rev.* **2003**, *27*, 145−163.
(6) Singh, V. K.; Xiong, A.; Usgaard, T. R.; Chakrabarti, S.; Deora, R.; Misra, T. K.; Jayaswal, R. K. *Mol. Microbiol.* **1999**, *33*, 200−207.
(7) Kuroda, M.; Hayashi, H.; Ohta, T. *Microbiol. Immunol.* **1999**, *43*, 115−125.
(8) Moore, C. M.; Helmann, J. D. *Curr. Opin. Microbiol.* **2005**, *8*, 188−195.
(9) Lee, S. M.; Grass, G.; Haney, C. J.; Fan, B.; Rosen, B. P.; Anton, A.; Nies, D. H.; Rensing, C. *FEMS Microbiol. Lett.* **2002**, *215*, 273−278.
(10) Eicken, C.; Pennella, M. A.; Chen, X.; Koshlap, K. M.; VanZile, M. L.; Sacchettini, J. C.; Giedroc, D. P. *J. Mol. Biol.* **2003**, *333*, 683−695.
(11) Pennella, M. A.; Shokes, J. E.; Cosper, N. J.; Scott, R. A.; Giedroc, D. P. *Proc. Natl. Acad. Sci. U.S.A.* **2003**, *100*, 3713−3718.

metal ion binding triggers a quaternary conformational change, which decreases the binding affinity of SmtB for the *smt* operator.[10,12] This quaternary structural switch in SmtB is mediated by an intersubunit hydrogen bonding network that originates with the nonliganding $N^{\epsilon 2}$ face of H117 (homologous to H97 in CzrA), which stabilizes a low-affinity DNA-binding conformation. Interestingly, the crystal structure of Zn_1-SmtB revealed that this structure was identical to that of apo-SmtB, suggesting that both metal binding sites had to be occupied to drive the structural switch.[10] In contrast to SmtB, the extent of Zn(II) occupancy in CzrA required to trigger a quaternary structural switch is unclear, since the X-ray structures of apo- and Zn_2-CzrA are largely superimposable,[10] a finding partly explained by crystal packing. In solution, however, the conformational dynamics of CzrA become markedly dampened on Zn(II) binding, suggesting that Zn(II) saturation might "freeze out" a low affinity DNA binding form of CzrA. The extent to which occupancy of both Zn(II) sites in homodimeric CzrA is required for rigidification of the dimer is unknown.

The exquisite Zn(II)/Co(II) specificity and the proposed quaternary structural change in CzrA upon metal binding make CzrA a promising candidate for the development of protein-based sensing device for these metal ions. Introduction of a fluorescence donor and acceptor into each of the two subunits could be used to detect the presence of Zn(II) or Co(II) at picomolar concentrations by monitoring the change in FRET efficiency upon metal ion binding. However, the homodimeric nature of CzrA requires that the instability originating with the monomer−dimer equilibrium ($K_{dimer} = 1.7 \times 10^5\ M^{-1}$)[11] and the inability to selectively label a single specific residue in the homodimer be overcome. To overcome these complications, recombinant genes containing two copies of the *czrA* coding region connected by 15, 30, or 45 nucleotide inserts encoding $(\text{-Gly}_4\text{Ser}_1\text{-})_n$ ($n = 1$, 2, or 3) repeats[13−20] (Figure 1A) have been constructed with the resulting proteins, designated 5L-, 10L- and 15L-fCzrA, respectively, purified, and characterized. A systematic investigation into the influence of linker length on the structure and function of CzrA seemed particularly important since the allosteric metal sites are near the C-terminus, close to where the peptide linker would be introduced. In addition, we reasoned that such an approach might provide a "molecular ruler" to probe quaternary structural changes that are required for metal binding, DNA binding, and allosteric coupling of the two.

For an eventual biosensor application, the fused proteins must preserve or improve the unique properties of the wild-type protein. In this work, we show that single-chain fused dimers of CzrA can indeed be created that preserve the structure and function of homodimeric CzrA, but these properties are strongly dependent on linker length. We further exploit the fused dimer

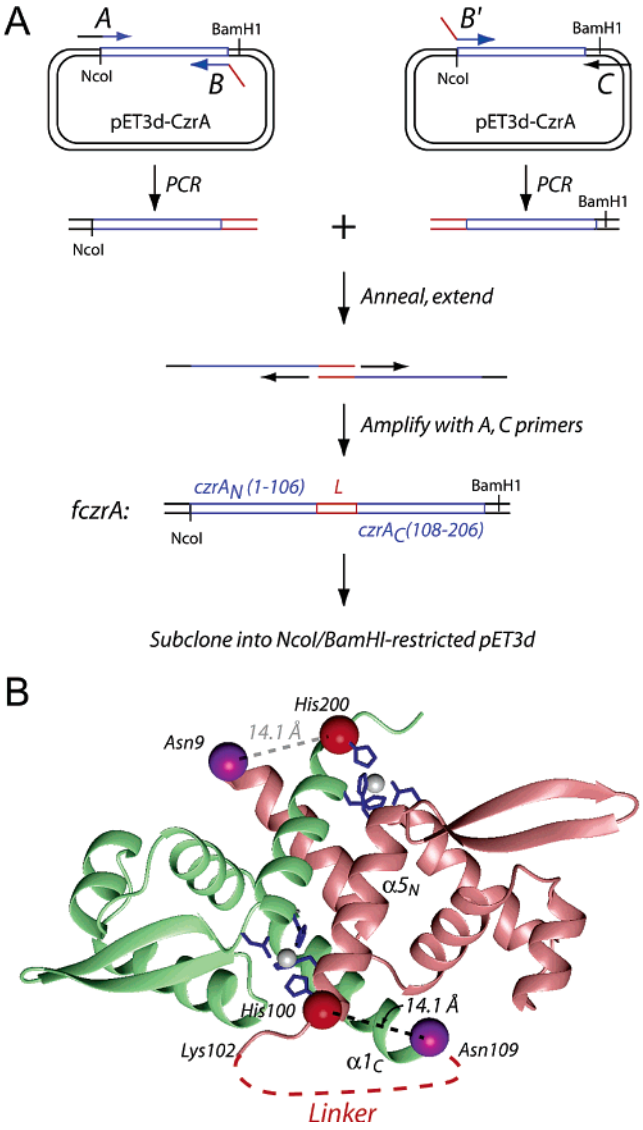

Figure 1. (A) Scheme for construction of an overexpression plasmid encoding various fCzrAs. The red-colored regions of PCR primers B and B′ are complementary and encode either a 5- or 10-amino acid linker, while eliminating the *Bam*HI and termination codons (primer B) and the *Nco*I site and codons 1−7 (primer B′) from the upstream and downstream *czrA* genes in the *fCzrA* gene array, respectively (see Experimental Section for more details). (B) Ribbon representation of the structure of Zn_2 CzrA,[10] with the linear Cα−Cα distance indicated (broken line) between His100 (red sphere) of the salmon protomer (arbitrarily designated the N-terminal protomer domain in fCzrA, numbered 1−106) and Asn9 (purple sphere, labeled Asn109) of the green protomer (designated the C-terminal protomer domain where residues 8−106 are denoted 108−206). The α5 Zn(II) ions are shown (grey spheres) as are the Zn(II)-coordinating ligands (shaded blue). The α5 metal sites are arbitrarily referred to as site 1 (Asp84, His86, His197, His200) and site 2 (His97, His100, Asp 184, His186) with metal site 2 proximate to the $(\text{Gly}_4\text{−Ser})_n$ linker in fCzrAs. The figure was prepared with MOLMOL.[54]

system to selectively abrogate formation of one of the two symmetry-related tetrahedral metal chelates in the dimer, to directly determine the degree to which occupancy of both metal sites in CzrA is required to drive allosteric regulation of CzrO[21]

(12) VanZile, M. L.; Chen, X.; Giedroc, D. P. *Biochemistry* **2002**, *41*, 9776−9786.
(13) Ladurner, A. G.; Fersht, A. R. *J. Mol. Biol.* **1997**, *273*, 330−337.
(14) Jana, R.; Hazbun, T. R.; Fields, J. D.; Mossing, M. C. *Biochemistry* **1998**, *37*, 6446−6455.
(15) Krueger, C.; Berens, C.; Schmidt, A.; Schnappinger, D.; Hillen, W. *Nucleic Acids Res.* **2003**, *31*, 3050−3056.
(16) Sieber, M.; Allemann, R. K. *Nucleic Acids Res.* **1998**, *26*, 1408−1413.
(17) Sieber, M.; Allemann, R. K. *Nucleic Acids Res.* **2000**, *28*, 2122−2127.
(18) Hallewell, R. A.; Laria, I.; Tabrizi, A.; Carlin, G.; Getzoff, E. D.; Tainer, J. A.; Cousens, L. S.; Mullenbach, G. T. *J. Biol. Chem.* **1989**, *264*, 5260−5268.
(19) Toth, M. J.; Schimmel, P. *J. Biol. Chem.* **1986**, *261*, 6643−6646.
(20) Bizub, D.; Weber, I. T.; Cameron, C. E.; Leis, J. P.; Skalka, A. M. *J. Biol. Chem.* **1991**, *266*, 4951−4958.

(21) Abbreviations used: *czr*, chromosomal zinc regulation; CzrA, also referred to as *S. aureus* ZntR in strain RN450;[35] fCzrA, fused CzrA; mag-fura-2, 2-[6-[bis(carboxymethyl)amino]-5-(carboxymethoxy)-2-benzofuranyl]-5-oxazolecarboxylic acid; CzrO, *czr* operator; quin-2, *N*-(2-((8-(bis(carboxymethyl)amino)-6-methoxy-2-quinolinyl)methoxy)-4-methylphenyl)-*N*-(carboxymethyl)glycine.

binding. We show that occupancy of a single metal site contributes ~69−83% of the total heterotropic allosteric coupling free energy (ΔG_c), reflective of significant metal-loregulation of DNA binding. In future work, we will exploit the fused CzrA (fCzrA) design to introduce single cysteine residue(s) within individual protomer domains for facile labeling with appropriate fluorescent[22,23] or redox-sensitive[24,25] probes for reagentless biosensing[26] or other applications.[27]

Results

Design of fused dimers of *S. aureus* CzrA. The $(Gly_4Ser)_n$ peptide linker in fused CzrAs (fCzrA) connects Leu106, the C-terminal residue of the N-terminal protomer domain, to Ile8′ of the C-terminal protomer domain (designated Ile108 in fCzrAs) (Figure 1B). The crystallographic structures of both apo- and Zn_2-CzrA reveal that residues 1−8 and 101 (or 102)−106 are not visible in the electron density maps, suggesting that they are disordered in both conformations.[10] Chemical shift indexing[4] and the magnitude of the $^1H-^{15}N$ heteronuclear NOE (unpublished results) suggest that this is the case in solution as well. As a result, the choice of connecting point between the N- and C-terminal protomer domain in fCzrAs is somewhat arbitrary, but the available data suggest that residues 1−7 are disordered and dispensable for repressor function. To directly demonstrate this, we purified a deletion mutant of CzrA in which most of the N-terminal unstructured region (residues 3−9, which joins Met1-Ser2 with Thr10) was deleted. This mutant, CzrA-(Δ3−9), possesses Co(II), Zn(II), and DNA binding properties that are indistinguishable from that of *wt*-CzrA (see Figures S1−S3 in the Supporting Information). Thus, the particular properties of individual fCzrAs characterized here derive exclusively from introduction of the covalent tether and not from deletion of residues 1−7 in the second protomer domain.

The Cα−Cα distance between His100 (the last residue in the C-terminal α5 helix and a metal ligand) and Asn9′ (the N-terminal residue in the α1 helix of the other protomer) is 14.1 Å in apo-CzrA (Figure 1B). Since the distance between the Cα of Leu106 to the Cα of serine in a single Gly_4Ser linker is 17.5 Å in a fully extended chain (3.5 Å per residue),[28] even the shortest linker used in this study should be capable of connecting Leu106 of one protomer and Ile8′ of the other, particularly since the C-terminal residues 102−106 and Ile8′ are disordered in both forms of the protein.[10] A more realistic estimate of the linker-spanning distance is to consider the linker as a "random walk" chain;[29] in this case, the mean end-to-end distance, $\langle r \rangle$, falls to 8.5 Å for the Gly_4Ser linker in 5L-fCzrA (assuming a length of each virtual Cα−Cα bond of 3.8 Å and a chain length, *n*, of 5 residues) and 12.6 Å between Lys102 and Ile108 ($n = 11$) (see Figure 1B). For 10L- and 15L-fCzrAs, $\langle r \rangle$ increases to 12.0 Å for the linker alone (15.2 Å for $n = 16$) and 14.7 Å (17.5 Å for $n = 21$), respectively.

Previous investigations of the effect of linker length, *n*, on protein stability generally reveal an inverse correlation between linker length and protein stability, qualitatively in accord with predictions from a simple loop entropy model from polymer theory.[13,29,30] The analysis of equilibrium urea denaturation curves obtained for the metal-free *wt*-CzrA vs 5L-, 10L-, and 15L-fCzrAs with a simple two-state unfolding model is largely consistent with this picture (Figure S4, Supporting Information). All fCzrAs are characterized by $[urea]_{1/2}$ values greater than untethered *wt*-CzrA, as anticipated from removal of the monomer−dimer equilibrium from the unfolding equilibria in fCzrAs.[14] 5L- and 10L-fCzrAs have conformational stabilities ($\Delta G(H_2O)$) of 8.1 and 7.9 kcal mol^{-1}, both ≥1.0 kcal mol^{-1} larger than *wt*-CzrA, while 15L-fCzrA is destabilized such that ($\Delta G(H_2O)$ is comparable to that of unfused *wt*-CzrA (12 μM monomer; 6.9 kcal mol^{-1}). In any case, introduction of the covalent linker in no case results in a large perturbation of the structure and stability of the apo-homodimers.

Structures of the metal binding sites are unperturbed in the fCzrAs. The metal binding sites of wild-type homodimeric CzrA (denoted *wt*-CzrA) adopt tetrahedral coordination geometries as revealed first by Zn(II)-EXAFS and visible absorption spectra of the Co(II)-substituted derivative,[11] and subsequently by X-ray crystallography.[10] The visible absorption spectrum and the extinction coefficient at 570 nm, $\epsilon_{570} = 900$ (±40) $M_{homdimer}^{-1}$ cm^{-1} for Co(II)-*wt*-CzrA (see Figure 2A), are identical to those previously reported,[11] diagnostic of a four-coordinative environment with tetrahedral or distorted tetrahedral coordination geometry around the Co(II) ions.[31] 10L-fCzrA and 15L-fCzrA also show the same Co(II) absorption spectra as *wt*-CzrA, except for the slightly reduced apparent molar absorptivities at 570 nm of 810 (±10) M^{-1} cm^{-1} and 845 (±15) M^{-1} cm^{-1}, respectively. The Co(II) binding isotherms shown in Figure 2B for 10L-fCzrA and 15L-fCzrA reveal the expected stoichiometry of two Co(II) binding sites per fCzrA molecule, revealing that the 10- and 15-amino acid linkers do not greatly distort the structures and apparent stoichiometries of metal binding in fCzrAs.

The Co(II) absorption spectrum for 5L-fCzrA shows the same spectral shape as that of *wt*-CzrA, but with approximately one-half the molar absorptivity, $\epsilon_{570} \approx 450$ (±50) M^{-1} cm^{-1}, of *wt*-CzrA, consistent with only a single functional Co(II) binding site on this fused dimer. This is confirmed by a stoichiometric titration (Figure 2B). This suggests that the 5-amino acid linker may be too short to span the required distance between the α5 and α1′ helices of the N- and C-terminal protomer domains in the Zn(II)-saturated conformation, with one of the α5 metal binding sites essentially inactivated ($K_{Co} \leq 10^4$ M^{-1}). In contrast, the remaining α5 metal site in 5L-fCzrA clearly has a wild-type coordination environment and a high affinity for Co(II).

Zn(II) binding properties of fCzrA are strongly dependent on linker length. The Co(II)-binding isotherms (Figure 2B) show essentially stoichiometric binding of Co(II) under these solution conditions, i.e., $K_{Co} > 10^7$ M^{-1}. Since Zn(II) is expected to bind 10^3-10^4-fold more tightly,[32] chelator competition experiments[10,33] were carried out in order to determine the stepwise affinities, K_{Zn1} and K_{Zn2}, to successive metal sites on

(22) Wu, P.; Brand, L. *Anal. Biochem.* **1994**, *218*, 1−13.
(23) Ratner, V.; Kahana, E.; Eichler, M.; Haas, E. *Bioconjugate Chem.* **2002**, *13*, 1163−1170.
(24) Benson, D. E.; Conrad, D. W.; de Lorimier, R. M.; Trammell, S. A.; Hellinga, H. W. *Science* **2001**, *293*, 1641−1644.
(25) Sandros, M. G.; Gao, D.; Benson, D. E. *J. Am. Chem. Soc.* **2005**, *127*, 12198−12199.
(26) Dattelbaum, J. D.; Looger, L. L.; Benson, D. E.; Sali, K. M.; Thompson, R. B.; Hellinga, H. W. *Protein Sci.* **2005**, *14*, 284−291.
(27) Zhang, Z.; Rajagopalan, P. T.; Selzer, T.; Benkovic, S. J.; Hammes, G. G. *Proc. Natl. Acad. Sci. U.S.A.* **2004**, *101*, 2764−2769.
(28) Stryer, L. *Biochemistry*, 4th ed.; Freeman: New York, 1995; pp 28−32.
(29) Wang, L.; Rivera, E. V.; Benavides-Garcia, M. G.; Nall, B. T. *J. Mol. Biol.* **2005**, *353*, 719−729.
(30) Nagi, A. D.; Regan, L. *Folding Des.* **1997**, *2*, 67−75.
(31) Corwin, D. T.; Fikar, R.; Koch, S. A. *Inorg. Chem.* **1987**, *26*, 3079−3080.
(32) VanZile, M. L.; Cosper, N. J.; Scott, R. A.; Giedroc, D. P. *Biochemistry* **2000**, *39*, 11818−11829.

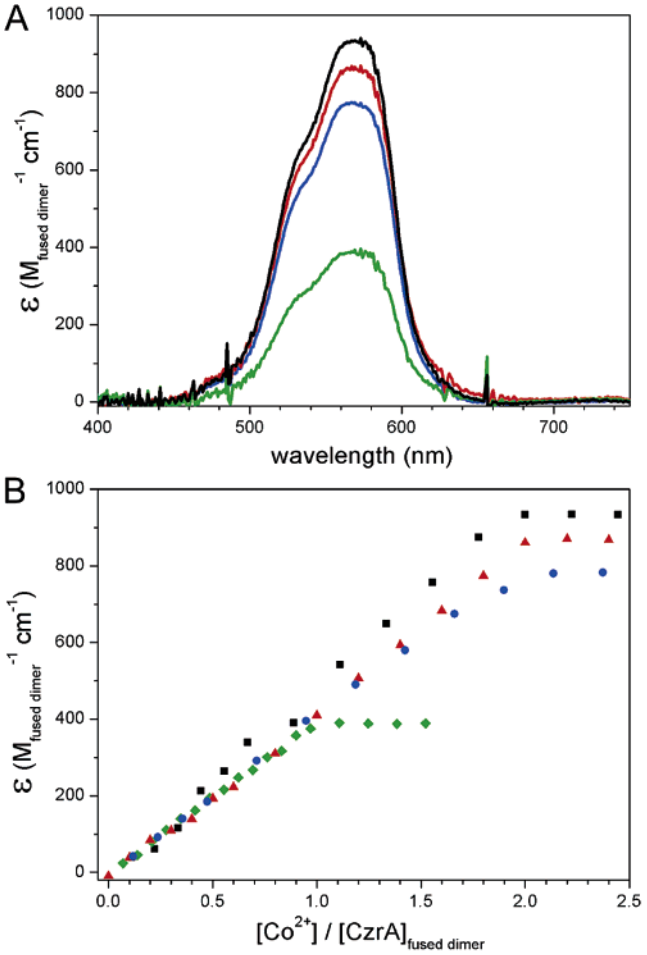

Figure 2. (A) Corrected UV−visible electronic absorption spectra of Co(II)-saturated (2.2 molar dimer equiv of total Co(II) added) *wt*-CzrA homodimer (black continuous line), 15L-fCzrA (red), 10L-fCzrA (blue), and 5L-fCzrA (green). (B) Molar absorptivities are calculated per mol dimer equiv of Co(II) binding isotherms plotted as corrected absorbance at 570 nm vs molar dimer equivalents of total Co(II) added for *wt*-CzrA homodimer (black), 15L-fCzrA (red), 10L-fCzrA (blue), and 5L-fCzrA (green). Conditions: 35−50 μM dimer, 10 mM Hepes, 0.4 M NaCl, pH 7.0, 22 °C.

the fused CzrA dimer. Figure 3 shows the representative Zn(II) binding isotherms obtained with the competitor chelator quin-2 (K_{Zn} = 2.7 × 10^{11} M^{-1} at pH 7.0) for *wt*-, 15L-, 10L-, and 5L-fCzrAs. Zn(II) binding to *wt*-CzrA is characterized by strong negative cooperativity with K_{Zn1} = 2.5 (±0.3) × 10^{12} M^{-1} greater than K_{Zn2} = 3.4 (±0.6) × 10^{10} M^{-1}, as found previously.[10] This gives a macroscopic (overall) Zn(II) binding affinity of $A_{Zn2} = K_{Zn1}{\cdot}K_{Zn2}$ = 8.5 × 10^{22} M^{-2}. Individual K_i can also be cast in terms of a single site binding constant, k, and a cooperativity parameter, ω, from $K_{Zn1} = 2{\cdot}k$ and $K_{Zn2} = \omega k/2$, yielding k = 1.3 × 10^{12} M^{-1} and ω = 0.054, or strong negative homotropic cooperativity (Table 1). The free energy of homotropic coupling of Zn(II) binding, ΔG^{Zn}_c, is simply given by

$$\Delta G^{Zn}_c = -RT{\cdot}\ln\omega$$

For *wt*-CzrA, ΔG^{Zn}_c = +1.7 kcal mol^{-1}. The N-terminal deletion mutant, CzrA(Δ3−9), is characterized by Zn(II) binding properties that are nearly indistinguishable from *wt*-CzrA (Figure

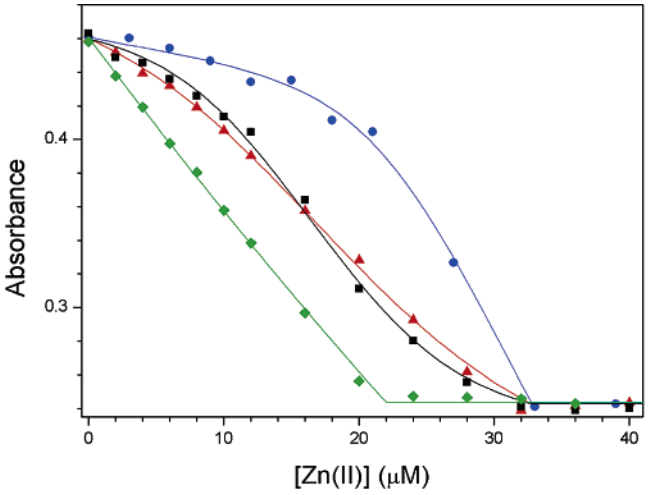

Figure 3. Representative quin-2-apo-CzrA competition Zn(II) binding isotherms obtained for apo *wt*-CzrA (black squares), 15L-fCzrA (red triangles), 10L-fCzrA (blue circles), and 5L-fCzrA (green diamonds) (see Experimental Section). Conditions: [fCzrA] = 10 μM or 20 μM *wt*-CzrA monomer and [Quin-2] = 12 μM, 10 mM Hepes, 0.4 M NaCl, pH 7.0, 22 °C. The continuous lines through each set of data represent a nonlinear least-squares fit of the change in quin-2 absorbance at 265 nm to two-step metal-binding model for *wt*-CzrA (black), 15L-fCzrA (red), 10L-fCzrA (blue), and 5L-fCzrA (green), respectively. K_{Zn1} and K_{Zn2} were resolved from this analysis as follows: *wt*-CzrA, K_{Zn1} = 2.5 (±0.3) × 10^{12} M^{-1}, K_{Zn2} = 3.4 (±0.6) × 10^{10} M^{-1}; 15L-fCzrA, K_{Zn1} = 1.3 (±0.1) × 10^{12} M^{-1}, K_{Zn2} = 7.2 (±0.7) × 10^{10} M^{-1}; 10L-fCzrA, K_{Zn1} = 3.0 (±1.6) × 10^{12} M^{-1}, K_{Zn2} = 2.7 (±0.9) × 10^{12} M^{-1}; 5L-fCzrA, K_{Zn1} = 2.3 (±0.1) × 10^{11} M^{-1}.

S2, Supporting Information) (Table 1). Like *wt*-CzrA, Zn(II) binding to 15L-fCzrA shows the same trend in negative cooperativity with K_{Zn1} = 1.3 (±0.1) × 10^{12} M^{-1} and K_{Zn2} = 7.2 (±0.7) × 10^{10} M^{-1} (A_{Zn2} = 9.5 × 10^{22} M^{-2}; k = 6.5 × 10^{11} M^{-1} and ω = 0.23), although ω is measurably larger than that of unfused *wt*-CzrA, which reduces ΔG^{Zn}_c to +0.9 kcal mol^{-1} (Table 1).

Strikingly, 10L-fCzrA is characterized by two large stepwise affinities with $K_{Zn1} \approx K_{Zn2}$ since K_{Zn1}= 3.0 (±1.6) × 10^{12} M^{-1} and K_{Zn2} = 2.7 (±0.9) × 10^{12} M^{-1}.[10] This gives A_{Zn2} = 8.1 × 10^{24} M^{-2} or 100-fold tighter than *wt*-CzrA (Table 1). In fact, if one assumes that both binding sites within the fused dimer have identical intrinsic affinities, then k = 1.5 × 10^{12} M^{-1} and ω = 3.6, indicative of slightly *positively* cooperative Zn(II) binding (ΔG^{Zn}_c = −0.8 kcal mol^{-1}) (Table 1). Finally, as expected, 5L-fCzrA exhibits only one high affinity metal binding site, K_{Zn1} = 2.3 (±0.1) × 10^{11} M^{-1} or ∼10-fold lower than K_{Zn1} for *wt*-CzrA, with an upper limit for K_{Zn2} of 10^5 M^{-1} derived from parallel mag-fura-2 titrations (data not shown).[10]

The origin of this change in sign in homotropic cooperativity of Zn(II) binding to unfused *wt*-CzrA vs 10L-fCzrA was further investigated by NMR spectroscopy. Full $^1H-^{15}N$ spectra of *wt*-CzrA and 10L-fCzrA were acquired in the absence of metal (apo; blue cross-peaks), in the presence of a single molar dimer equiv (Zn_1; green cross-peaks) and with 2 molar dimer equiv (Zn_2; red cross-peaks) of Zn(II), and the resulting spectra superimposed on one another (see Figures S5 and S6, respectively, in the Supporting Information). Selected regions of these spectra that highlight various amide resonances from residues distributed throughout the molecule, most of which are characterized by a large change in chemical shift and/or H−D exchange rate,[10] are shown in Figure 4 for *wt*-CzrA (panels

(33) VanZile, M. L.; Chen, X.; Giedroc, D. P. *Biochemistry* **2002**, *41*, 9765−9775.

Table 1. Equilibrium Stepwise K_{Zn1}, Macroscopic (A_1) and Site (k, ω) Zn(II) Binding Constants of Individual CzrA Derivatives

parameter	*wt*-CzrA	CzrA(Δ3-9)	15L-fCzrA	10L-fCzrA	5L-fCzrA
K_{Zn1} (M^{-1})[a]	2.5 (±0.3) × 10^{12}	2.1 (±0.5) × 10^{12}	1.3 (±0.1) × 10^{12}	3.0 (±1.6) × 10^{12}	2.5 (±0.3) × 10^{12}
K_{Zn2} (M^{-1})[a]	3.4 (±0.6) × 10^{10}	4.9 (±1.2) × 10^{10}	7.2 (±0.7) × 10^{10}	2.7 (±0.9) × 10^{12}	<10^{5}
A_{Zn2} (M^{-2})[b]	8.5 (±0.7) × 10^{22}	1.0 (±1.3) × 10^{23}	9.5 (±0.7) × 10^{22}	8.1 (±1.8) × 10^{24}	<2.5 (±0.3) × 10^{17}
k (M^{-1})[c]	1.3 (±0.2) × 10^{12}	1.1 (±0.3) × 10^{12}	6.5 (±0.5) × 10^{11}	1.5 (±0.8) × 10^{12}	1.3 (±0.2) × 10^{12}
ω	0.054 (±0.023)	0.093 (±0.062)	0.23 (±0.06)	3.6 (±2.6)	
ΔG^{Zn}_{c} (kcal mol^{-1})[d]	+1.7 (±0.2)	+1.4 (±0.4)	+0.9 (±0.2)	−0.8 (±0.4)	

[a] Derived from a stepwise Zn(II)-binding model from experiments like that shown in Figure 3.[10] [b] $A_{Zn2} = K_{Zn1}\cdot K_{Zn2}$. [c] Derived from $K_{Zn1} = 2\cdot k$ and $K_{Zn2} = \omega k/2$. [d] $\Delta G^{Zn}_{c} = -RT\cdot\ln\omega$.

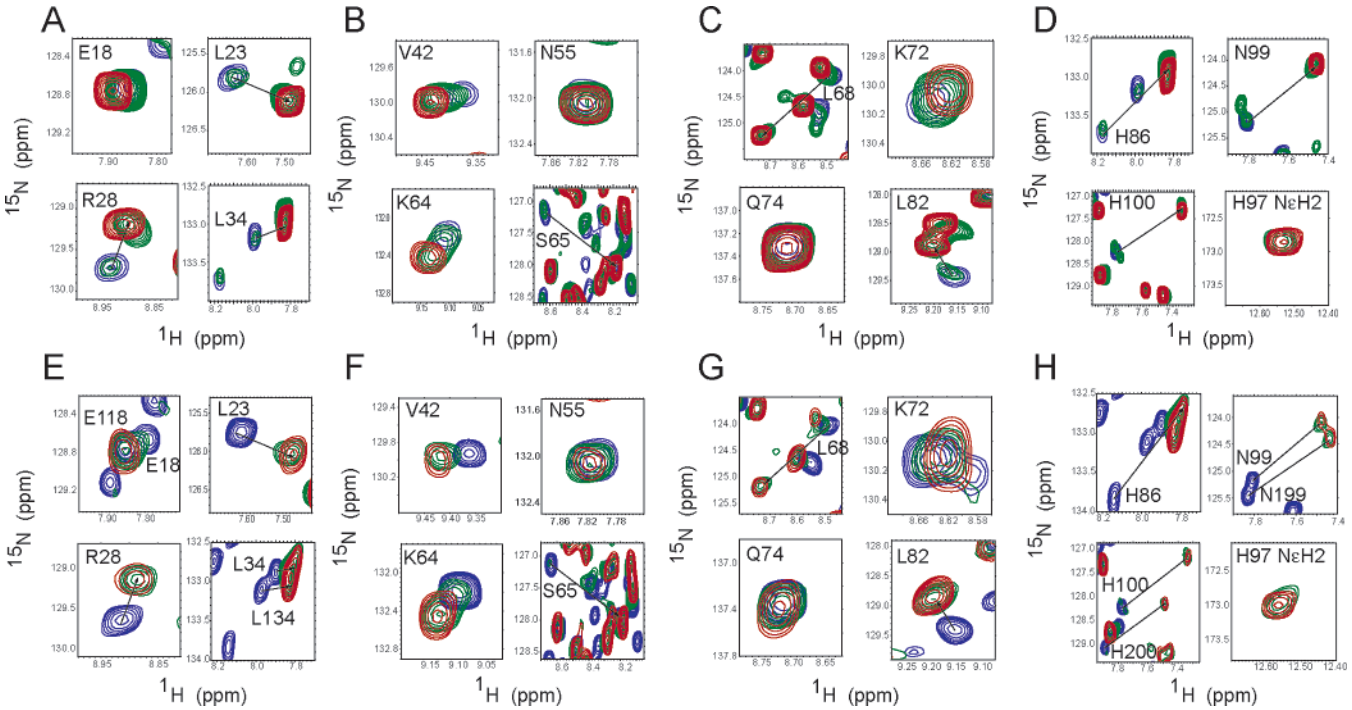

Figure 4. Selected regions of superimposed $^{1}H-^{15}N$ HSQC spectra acquired for *wt*-CzrA homodimer (panels A−D) and 10L-fCzrA (panels E−H) in the absence of added Zn(II) (blue cross-peaks) and addition of 1.0 dimer molar equiv of Zn(II) (green contours) and 2.0 dimer molar equiv of Zn(II) (red cross-peaks). (A, E) Resonances derived from the α1 (E18, L23, R28) and α2 helices (L34). (B, F) Cross-peaks corresponding to residues in the α3 (V42) and αR (N55, K64, S65) helices. (C, G) Resonances from the turn region between α4 and β1 (L68) and the β1 (K72, Q74)-β2 (L82) hairpin. (D, H) Resonances from the C-terminal α5 helix, including two Zn(II) ligands (H86, H100) and the H97 $NH^{\epsilon 2}$ side chain correlation.

A−D) and 10L-fCzrA (panels E−H). For *wt*-CzrA, the spectrum of Zn_1 *wt*-CzrA (green) is characterized by a superposition of apo-like (blue) and Zn_2 (red) protomer conformations in slow exchange on the NMR time scale. This includes amide correlations for residues distant from the Zn(II) coordination site (panels A−C), as well as in the α5 helix itself (panel D). Most importantly, the His97 $NH^{\epsilon 2}$ correlation, previously implicated in the formation of the cross-subunit hydrogen bond important for allosteric switching[10] is also clearly present in the spectrum of Zn_1 *wt*-CzrA. Since the extent of negative cooperativity ensures that the dominant ligand-bound, homodimeric species will have a single Zn(II) ion bound to one α5 metal site with the other symmetry-related site empty, these spectra reveal that the binding of a single metal induces structural asymmetry into the dimer, effectively switching just one-half of the protomers to a Zn_2-like conformation. The quaternary structural conformational transition is then completed with the binding of the second Zn(II) to the homodimer.

In contrast to *wt*-CzrA, the spectra of 10L-fCzrA show that the dominant conformation of 10L-fCzrA in the presence of 1 molar equiv of Zn(II) is that of a nearly fully quaternary structurally switched dimer, since, for the majority of amide correlations, there is far less "apo-like" (green superimposed on blue) cross-peak intensity relative to Zn_2-like (green superimposed on red) cross-peaks than can be accounted for on the basis of the fractional occupancy of the protomer domains ($\Theta = 0.5$). Although there are exceptions (e.g., K64), this is even true for resonances in the α5 (e.g., N99, H100) and α1/α2 helices (E18, L34) that exhibit peak doubling in the apoprotein due to the linker which breaks the symmetry of the fused dimer. These spectra therefore suggest a structural rationale for the loss of negative cooperativity of Zn(II)-binding in 10L-fCzrA: the 10-residue linker might bias the conformational ensemble of apo-CzrA such that the energy separation between a highly populated apo- and weakly populated Zn_2-like quaternary states is smaller.[34] In this case, much of the energetic penalty that must be paid to switch the remaining protomer in the fused dimer has been paid by the linker; this in turn leads to slightly positively cooperative binding to the two metal sites in 10L-fCzrA.

DNA binding properties of fCzrAs. The results from the above experiments reveal that both 15L- and 10L-fCzrAs bind 2 molar equiv of Co(II) or Zn(II) per dimer as expected, with distinct homotropic Zn(II)-binding cooperativities; in contrast,

(34) Mulder, F. A.; Mittermaier, A.; Hon, B.; Dahlquist, F. W.; Kay, L. E. *Nat. Struct. Biol.* **2001**, *8*, 932−935.

5L-fCzrA binds a single equivalent of metal with high affinity. It was next of interest to determine the extent to which Zn(II)-binding negatively allosterically regulates CzrO binding by fCzrAs.[11]

Figure 5 shows the results of multiple independent fCzrA binding experiments carried out by monitoring the change in the anisotropy of the fluorescence of either a 57-bp fluorescein-labeled CzrO fragment used previously[11] (Figure 5A−C) or a 41-bp Cy3-labeled DNA (Figure 5A,D), with all K_i compiled in Table 2. The 57-bp oligonucleotide contains the entire region of the *czr* operator-promoter region footprinted by CzrA, denoted CzrO,[35] while the 41-bp fragment lacks the downstream half of the second overlapping 12−2−12 imperfect inverted repeat (Figure 5A). As found previously for *wt*-CzrA, up to four homodimers can be bound under these relatively high salt conditions,[11] consistent with a stoichiometry of two homodimers per 12−2−12 inverted repeat measured previously for apo-SmtB.[4,12] The K_i values resolved from analysis of the binding isotherms obtained with the 41-bp oligonucleotides are consistent with that of the longer oligonucleotide, exhibiting the same trends in K_i for each CzrA variant, except that K_3 is consistently 2−4-fold smaller and the binding of the fourth dimer is undetectable (Table 2); this is consistent with the sequences of each oligonucleotide (Figure 5A).

The first and the second *wt*-CzrA dimers bind to the 57-bp DNA very tightly with $K_1 = 2.7\ (\pm 0.5) \times 10^{10}\ M^{-1}$ and $K_2 = 3.2\ (\pm 0.5) \times 10^{9}\ M^{-1}$, with the third dimer binding affinity weaker, $K_3 = 3.7\ (\pm 0.5) \times 10^{7}\ M^{-1}$ (see Scheme 2, Experimental Section) (Table 2). Similar binding parameters were obtained for CzrA(Δ3−9) (Figure S4, Supporting Information), revealing that the N-terminal unstructured domain makes no contribution to DNA binding. For 15L-fCzrA, the first and second fused dimers bind to the 57-bp DNA ~20-fold weaker than *wt*-CzrA. Note, however, that the actual binding curve for *wt*-CzrA is positioned to the right relative to that for 15L-fCzrA, since the binding of homodimeric *wt*-CzrA is limited by the monomer−dimer equilibrium ($K_{dimer} = 1.7 \times 10^{5}\ M^{-1}$)[11] throughout the titration. For example, protein−DNA stoichiometries exceeding $(P_2)_2$·D complex are barely detected, and at low protein concentrations, the binding curve for *wt*-CzrA is sigmoidal (Figure 5B inset).

For 10L-fCzrA, all stepwise K_i's are further decreased by 4−10-fold relative to 15L-fCzrA with nearly identical trends observed for 5L-fCzrA as well (Figure 5C, Table 2), except that formation of the $(fP_2)_4$·D complex becomes too weak to detect for 10L- and 5L-fCzrAs. These data reveal that the intrinsic DNA binding affinities of apo forms of fCzrAs are strongly modulated by linker length. Of the three tethered fCzrAs, 15L-fCzrA binds DNA with an affinity closest to that of *wt*-CzrA, followed by 10L- and 5L-fCzrAs. It is important to note that the binding of all fCzrAs to the CzrO is sequence-specific since neither *wt*-CzrA nor 5L-fCzrA exhibit detectable binding to an unrelated 49-bp dsDNA under the same conditions (data not shown).

Saturating Zn(II) greatly decreases the CzrO binding affinity of all fused CzrAs, even for 5L-fCzrA, which binds a single equivalent of Zn(II) per dimer with high affinity (Figure 5B,C, open symbols).[36] Under these conditions, only a single fused dimer binds weakly to the DNA, with K_1 estimated to be 5.7 ×

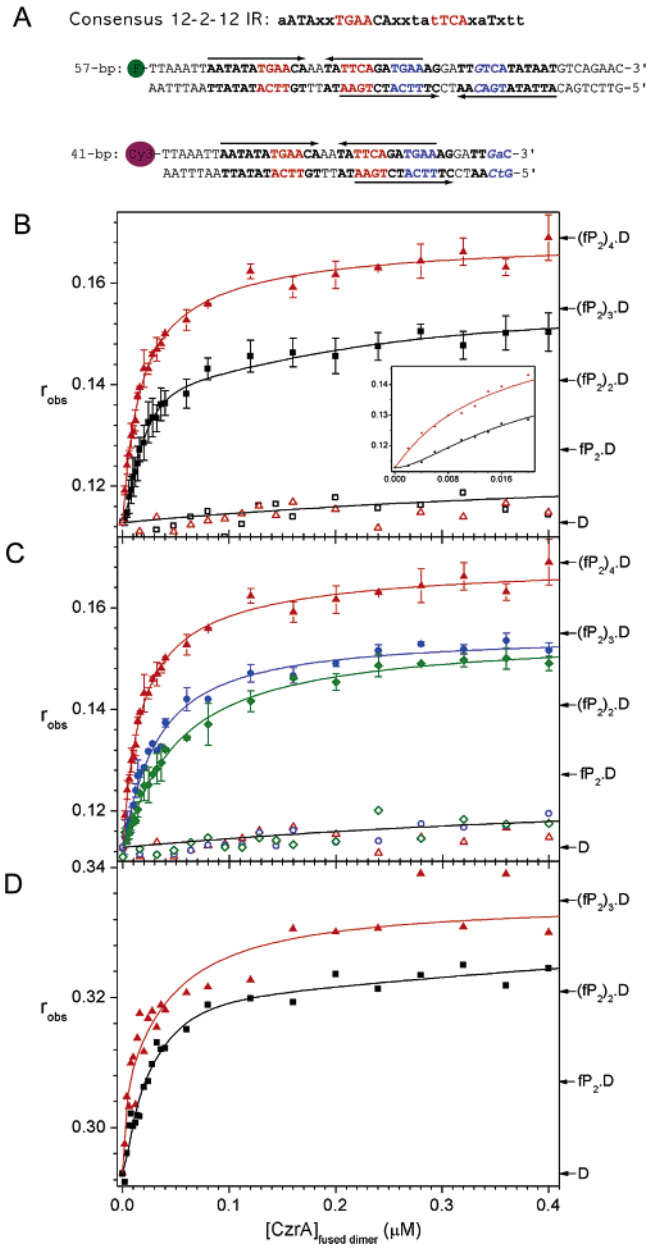

Figure 5. (A) Sequences of fluorescein-labeled 57-bp and Cy3-labeled 41-bp DNA oligonucleotides containing CzrO regions used in this study. The arrows designate two overlapping imperfect 12−2−12 inverted repeats that conform to the consensus 12−2−12 inverted repeat (IR) shown. (B) Fluorescence anisotropy-based binding isotherms obtained with a fluorescein-labeled 57-bp CzrO DNA and *wt*-CzrA (black squares) and 15L-fCzrA (red triangles) in the absence (filled symbols) and in the presence (open symbols) of $ZnSO_4$. (C) Fluorescence anisotropy-based binding isotherms obtained with a fluorescein-labeled 57-bp CzrO DNA and 15L-fCzrA (red triangles) and 10L-fCzrA (blue circles) and 5L-fCzrA (green diamonds) in the absence (filled symbols) and in the presence (open symbols) of $ZnSO_4$. (D) Representative fluorescence anisotropy-based binding isotherms obtained with a Cy3-labeled 41-bp CzrO DNA and *wt*-CzrA (black squares) and 15L-fCzrA (red triangles) in the absence of exogenously added $ZnSO_4$. The continuous lines through each data set represent a nonlinear least-squares fit to the sequential dimer-binding model outlined in Scheme 1 for fCzrAs and Scheme 2 for *wt*-CzrA homodimer (see Experimental Section). Data points with error bars represent the mean and standard errors from 3 to 4 independent experiments. Optimized K_i values from these fits are compiled in Table 2. Zn(II) pre-equilibrated and -saturated CzrA stocks ([fCzrA] = 10 μM or 20 μM *wt*-CzrA monomer with 25 μM $ZnSO_4$) were added to fluorescein-labeled DNA to obtain the DNA-Zn(II) CzrA binding isotherm. Conditions: 4 nM duplex DNA, 10 mM Hepes, 0.4 M NaCl, 100 μM EDTA (EDTA is not present in the metal−protein titrations), pH 7.0, 25.0 (±0.2) °C.

(35) Xiong, A.; Jayaswal, R. K. *J. Bacteriol.* **1998**, *180*, 4024−4029.

Table 2. Stepwise K_i and Associated Macroscopic (A_i) Equilibrium Binding Constants Resolved from Fluorescence Anisotropy-Based CzrO Binding Isotherms for Individual CzrA Derivatives

		wt-CzrA[a]	15L-fCzrA[b]	10L-fCzrA[b]	5L-fCzrA[b]	H97N;H197N 10L-fCzrA[b]
			Apoproteins			
57-bp DNA	K_1 ($\times 10^6$ M^{-1})	27400 ($\pm$5100)	1260 ($\pm$930)	108 ($\pm$28)	54.7 ($\pm$9.6)	460 ($\pm$210)
	K_2 ($\times 10^6$ M^{-1})	3220 ($\pm$490)	151 ($\pm$67)	39.6 ($\pm$11.0)	24.0 ($\pm$5.2)	148 ($\pm$55)
	K_1 ($\times 10^6$ M^{-1})	37.0 ($\pm$4.5)	43.3 ($\pm$16.0)	11.9 ($\pm$2.2)	6.3 ($\pm$0.9)	34.0 ($\pm$8.0)
	K_4 ($\times 10^6$ M^{-1})		8.7 ($\pm$1.7)			2.3 ($\pm$0.4)
	A_2 ($\times 10^{12}$ M^{-2})[c]	8.8 ($\pm$2.2) $\times 10^7$	1.9 ($\pm$1.6) $\times 10^5$	4300 ($\pm$1600)	1300 ($\pm$370)	6.8 ($\pm$4.0) $\times 10^4$
	A_3 ($\times 10^{18}$ M^{-1})[d]	3.3 ($\pm$1.4) $\times 10^9$	8.2 ($\pm$6.3) $\times 10^6$	5.1 ($\pm$2.1) $\times 10^4$	8300 ($\pm$2600)	2.3 ($\pm$1.5) $\times 10^6$
			Zn(II) Proteins			
	K_1 ($\times 10^6$ M^{-1})	0.57 ($\pm$0.12)	0.57 ($\pm$0.12)	0.57 ($\pm$0.12)	0.57 ($\pm$0.12)	6.0 ($\pm$1.0)
	K_2 ($\times 10^6$ M^{-1})	$\leq$0.1	$\leq$0.1	$\leq$0.1	$\leq$0.1	5.2 ($\pm$0.8)
	A_2 ($\times 10^{12}$ M^{-2})[e]	0.057	0.057	0.057	0.057	31 ($\pm$7.1)
	ΔG^1_c (kcal mol^{-1})[f]	6.3 ($\pm$0.2)	4.6 ($\pm$0.4) [73%]	3.1 ($\pm$0.2) [49%]	2.7 ($\pm$0.2) [43%]	2.6 ($\pm$0.3) [47%]
	ΔG^2_c (kcal mol^{-1})[g]	12.6 ($\pm$0.8)	8.9 ($\pm$0.8) [71%]	6.7 ($\pm$0.8) [53%]	5.9 ($\pm$0.8) [47%]	4.6 ($\pm$0.4) [37%]
			Apoproteins			
41-bp DNA[h]	K_1 ($\times 10^6$ M^{-1})	25300 ($\pm$6500)	2340 ($\pm$3400)	160 ($\pm$61)	54.1 ($\pm$28.0)	
	K_2 ($\times 10^6$ M^{-1})	1030 ($\pm$240)	43.9 ($\pm$20.0)	43.4 ($\pm$40.0)	23.9 ($\pm$14.0)	
	K_3 ($\times 10^6$ M^{-1})	4.9 ($\pm$1.7)	12.9 ($\pm$6.0)	5.4 ($\pm$5.4)	2.8 ($\pm$1.3)	
	A_2 ($\times 10^{12}$ M^{-2})	2.6 ($\pm$0.9) $\times 10^7$	1.0 ($\pm$1.6) $\times 10^5$	6900 ($\pm$6900)	1290 ($\pm$1000)	

[a] Calculated from fits obtained with the binding model outlined in Scheme 2 (see Experimental Section) with K_{dimer} fixed at 1.7×10^5 M^{-1}.[11] [b] Calculated from fits obtained with the binding model outlined in Scheme 1. [c] $A_2 = K_1 \cdot K_2$. [d] $A_3 = K_1 \cdot K_2 \cdot K_3$. [e] A_2 calculated assuming an upper limit of K_2 of 1.0×5 M^{-1}, values below which the fitted isotherm is insensitive. [f] $\Delta G^1_c = -RT \cdot \ln(K_1^{Zn(II)-CzrA}/K_1^{apo-CzrA})$, with the number in square brackets denoting % ΔG^1_c relative to unfused *wt*-CzrA. [g] $\Delta G^2_c = -RT \cdot \ln(A_2^{Zn(II)-CzrA}/A_2^{apo-CzrA})$, with the square brackets as defined above for ΔG^2_c. [h] Standard deviations of the fitted parameters are larger due to the small change in r_i upon CzrA binding (see Experimental Section).

10^5 M^{-1}. The free energy of allosteric coupling (ΔG_c) of Zn(II) and DNA binding by fCzrAs can be estimated from the following (eq 1):

$$\Delta G^1_c = -RT \cdot \ln(K_1^{Zn(II)-CzrA}/K_1^{apo-CzrA}) \qquad (1)$$

where ΔG^1_c is operationally defined as deriving from the first fCzrA-CzrO binding event only (i.e., K_1) since higher order complexes could not be observed for Zn(II)-saturated fCzrAs (Figure 5). ΔG^1_c for the *wt*-CzrA and CzrA(Δ3−9) homodimers are indistinguishable, 6.3 ($\pm$0.2) and 6.5 ($\pm$0.2) kcal mol^{-1} (Figure S4, Supporting Information), indicative of strong heterotropic allosteric negative coupling for the unfused dimers.[37] 15L-fCzrA is characterized by a ΔG^1_c of 4.6 ($\pm$0.4) kcal mol^{-1}, while ΔG^1_c values for 10L-fCzrA and 5L-fCzrA are 3.1 ($\pm$0.2) and 2.7 ($\pm$0.2) kcal mol^{-1}, respectively, or approximately half that of *wt*-CzrA (Table 2). Note, however, that this difference in ΔG^1_c is fully attributable to the lower DNA binding affinity of the respective apoproteins. Identical trends are observed in ΔG^2_c derived from the ratio of A_2 ($A_2 = K_1 \cdot K_2$) for Zn(II)-bound and apo CzrAs (see eq 1), calculated assuming an upper limit of 1×10^5 M^{-1} for K_2 for Zn(II) proteins (see Table 2).

Contribution of each metal site in 10L-fCzrA to ΔG_c is not additive. The DNA binding experiments presented above, particularly for 5L-fCzrA, make the prediction that just one of the two metal sites in fCzrAs is sufficient to induce significant allosteric regulation of *czr* O/P binding and that the two metal sites might not contribute in an additive fashion to ΔG_c. This is the expectation from the NMR experiments (see Figure 4) if filling of just one of the α5 metal sites, which creates significant quaternary structural asymmetry within the dimer, is capable of driving significant inhibition of DNA binding.

To directly test this proposal, we exploited the fused dimer system to introduce a single poorly metal liganding substitution into one of the two metal sites independently in the context of 10L-fCzrA.[37] Two 10L-fCzrA substitutions were prepared. These are denoted H97N 10L-fCzrA, which introduces the H97N mutation into the N-terminal protomer domain and perturbs metal site 2, closest to the peptide linker (see Figure 1B), and H197N 10L-fCzrA, which introduces the same substitution into the C-terminal protomer domain perturbing metal site 1, distant from the linker (see Figure 1B). An Asn substitution of His97 was chosen because previous work has shown that the H97N substitution in the context of the CzrA homodimer abrogates allosteric coupling ($\Delta G_c = 0$), and these metal sites adopt non-native coordination geometries and bind Zn(II) weakly ($K_{Zn1} = 6.8$ ($\pm$0.3) $\times 10^6$ M^{-1}; $K_{Zn2} \leq 1 \times 10^5$ M^{-1}) relative to *wt*-CzrA.[37] Thus, each substitution is expected to selectively disrupt just one of the His97-mediated H-bonding pathways linked to allostery since the critical $H^{\epsilon 2}$ proton is obviously not present in this mutant.[10]

Figure 6 shows representative fluorescence anisotropy-based CzrO binding isotherms (like those shown in Figure 5B,C) for H97N and H197N 10L-fCzrAs measured in the presence and absence of saturating Zn(II). The data obtained for each protein are superimposable and were therefore subjected to a simultaneous fit to the multiple-dimer binding model (see Scheme 1, Experimental Section). In the absence of Zn(II), the apoproteins bind with a $K_1 = 4.6$ ($\pm$2.1) $\times 10^8$ M^{-1} and $K_2 = 1.5$ ($\pm$0.6) $\times 10^8$ M^{-1}, a K_i similar to that of 15L-fCzrA but greater than that of the parent 10L-fCzrA (Figure 6; Table 2). In any case, K_1 and K_2 are reduced ~100-fold to 6.0 ($\pm$1.0) $\times 10^6$ M^{-1} and 5.2 ($\pm$0.8) $\times 10^6$ M^{-1}, respectively, in the presence of saturating Zn(II), yielding a ΔG^1_c of 2.6 ($\pm$0.3) kcal mol^{-1} and a ΔG^2_c of 4.6 ($\pm$0.4) kcal mol^{-1}. These values of ΔG^i_c are ~54% that of 15L-fCzrA but ≈77% that of the parent 10L-fCzrA and comparable to that of 5L-fCzrA, the latter of which can only bind a single equivalent of Zn(II) with high affinity. The magnitude of ΔG^i_c is independent of which metal site (1 or 2) is blocked, suggesting that the adjoining linker has little influence on allosteric coupling by metal site 2 in 10L-fCzrA.

(36) The 5L-fCzrA-CzrO complex also binds a single equivalent of Zn(II) with high affinity.
(37) Pennella, M. A.; Arunkumar, A. I.; Giedroc, D. P. *J. Mol. Biol.* **2006**, in press.

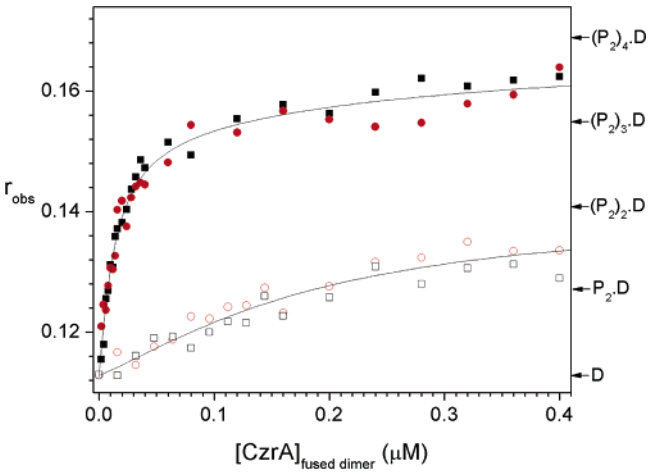

Figure 6. Representative fluorescence anisotropy-based binding isotherms obtained for fluorescein-labeled 57-bp DNA and H97N 10L-fCzrA (black squares) and His197N 10L-fCzrA (red circles) measured in the absence (filled symbols) and in the presence (open symbols) of $ZnSO_4$ in the binding reactions. Zn(II) pre-equilibrated and -saturated fCzrA stocks ([fCzrA] = 10 μM with [$ZnSO_4$] = 12 μM) were used to obtain the DNA-Zn(II) CzrA binding isotherm. The continuous lines through each data set represent a nonlinear least-squares fit to the sequential dimer-binding model outlined in Scheme 1. Optimized K_i values from these fits are compiled in Table 2. Conditions: 4 nM duplex DNA, 10 mM Hepes, 0.4 M NaCl, 100 μM EDTA (EDTA is not present in metal-protein titrations), pH 7.0, 25.0 (±0.2) °C.

The important point is, however, that occupancy of a single metal site in fCzrA, and presumably in homodimeric CzrA, is sufficient to regulate CzrO binding, promoting disassembly to a weakly bound $(fP_2)_2$·D species. This observation is in qualitative agreement with the DNA binding characteristics of 5L-fCzrA which binds a single Zn(II) ion as well (Figure 5; Table 2).

The conformational changes induced in H97N-10L-fCzrA upon sequential addition of 1 and 2 molar equiv of Zn(II) were further probed by NMR spectroscopy (Figure 7, compare panel A with Figure 4E,G and panel B with Figure 4H; see Figure S7, Supporting Information, for full spectra). Even though these spectra are complicated by a further break in the symmetry of the homodimer as a result of a single H97N substitution (cf., E18), they are qualitatively in accord with spectra of the parent 10L-fCzrA. Occupancy of the functional wild-type site 1 appears to induce quaternary structural switching of both protomer domains. Note that the hydrogen bonding pathway is also clearly established in the functional metal site as documented by the wild-type-like large shift in the amide correlation of Leu68 (Figure 7A) and the presence of the His97 $N^{\epsilon 2}-H^{\epsilon 2}$ cross-peak (Figure 7B).

Discussion

Single-chain fused CzrAs are functional for metal binding and DNA binding, but to varying degrees. In this work, we show that the C-terminal amino acid of one CzrA protomer can be covalently tethered to the N-terminal α1 helix of the other protomer via a $(Gly_4\text{-}Ser)_2$ or $(Gly_4\text{-}Ser)_3$ linker without large perturbations of the structure of the two tetrahedral metal-sensing Zn(II)/Co(II) binding sites. The CzrO binding properties and degrees of allosteric negative regulation of DNA binding by Zn(II) are, however, significantly effected even in these two fused dimers. The functional and structural properties of 15L-fCzrA containing a $(Gly_4\text{-}Ser)_3$ linker are closest to that of homodimeric *wt*-CzrA and collectively reveal that the $(Gly_4\text{-}Ser)_3$ linker, while not optimal with respect to DNA binding, readily spans the point-to-point distance associated with both the apo and Zn_2 forms of the homodimer in solution (Tables 1 and 2). In contrast, the DNA- and metal-binding properties of 10L-fCzrA, tethered by a $(Gly_4\text{-}Ser)_2$ linker, are easily distinguished from *wt*-CzrA (Tables 1 and 2). This linker length negatively influences not only DNA binding, limiting association of fCzrAs at all binding steps (Table 2),[38] but also Zn(II) binding, resulting in its strong negative homotropic cooperativity being lost and replaced with slightly positive cooperative binding (Figure 3; Table 1). Finally, the 5-residue linker in 5L-fCzrA likely induces significant strain even into the apo fused dimer, since one of the two metal binding sites is lost in this derivative (Figures 2 and 3). Although the origin of this effect is unknown, the fact that the molar ellipticities of 5L-, 10L-, and 15L-fCzrAs at 0 M urea are identical within experimental error (Figure S4, Supporting Information) rules out any large losses in α-helical structure in 5L-fCzrA relative to the other tethered derivatives.

Structural insight into these thermodynamic findings is provided by the $^1H-^{15}N$ HSQC spectra of *wt*-CzrA and 10L-fCzrA acquired as a function of the Zn(II) ligation state (Figure 4). As schematically illustrated in Figure 8A, the Zn_1 *wt*-CzrA homodimer is structurally asymmetric, with approximately half of the protomer domains switched to a Zn_2-like conformation, with the other protomer domain remaining in an apo-like conformation. Thus, the metal-induced quaternary structural/dynamical transition in CzrA is clearly not concerted in solution, in contrast to previous speculation.[10]

In contrast to *wt*-CzrA, filling half of the Zn(II) binding sites in 10L-fCzrA effectively switches both protomer domains to Zn_2-like conformations. Since the energetic penalty required to switch the other protomer domain does not have to be paid on binding the second Zn(II) ion, strong negative cooperativity of Zn(II) binding is abolished, leading to $K_{Zn1} \approx K_{Zn2}$ and a weakly positive cooperative binding of Zn(II) (Figure 3). One possible molecular explanation for this is that the 10-amino acid linker is not long enough to span the distance required to bridge the two protomer domains in the apoprotein, thus biasing the conformational ensemble toward a more "closed" Zn_2-like conformation (see Figure 8A, middle panel). In any case, the extent of the negative cooperativity of Zn(II) binding has little bearing on functional allosteric negative regulation of DNA binding by Zn(II), since the DNA-binding activity of 10L-fCzrA, while globally weaker than 15L-fCzrA, is regulated to the maximum extent possible by Zn(II) binding (Figure 5C).

We suggest that the lower affinities of both 10L- and 5L-fCzrA for the CzrO may originate with a shorter than optimal tether that connects the two protomer domains (see Figure 8B). This would restrict the movement of one protomer domain relative to the other upon DNA binding. It is currently unknown how the CzrA dimer binds to the CzrO, but two dimers can bind to a single 12−2−12 imperfect inverted repeat,[12,39] perhaps

(38) Determination of individual K_i in this complex coupled equilibrium (see Scheme 1) is dependent on an independent determination of the characteristic anisotropies r_i associated with each $(fP_2)_n$·D complex (see Experimental Section).[12] r_i values measured for 15L-fCzrA-CzrO complexes were used for complexes formed by all fCzrAs, a reasonable assumption provided the hydrodynamic properties of each complex are dictated by the number of fCzrAs bound, and not by large differences in DNA structure between analogous complexes. Since parallel titrations with a 41-bp Cy3-labeled dsDNA (Figure 5A) resolve identical K_i's (Table 2) despite vastly different r_i's, this assumption is likely valid.

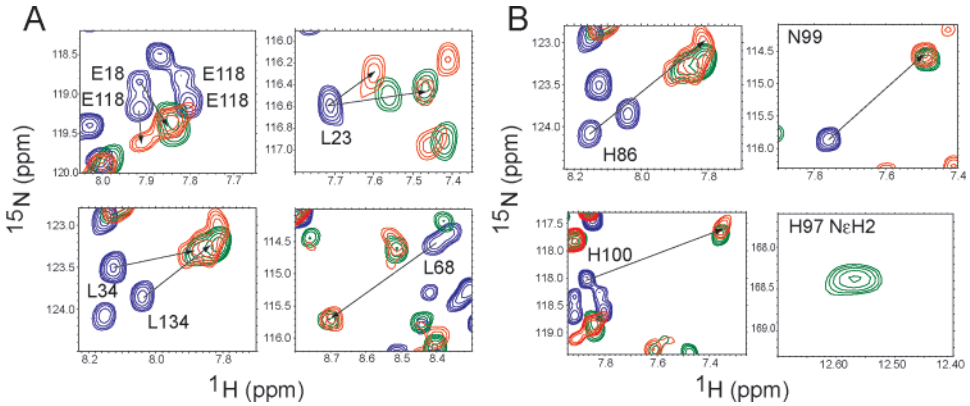

Figure 7. Selected regions of superimposed $^1H-^{15}N$ HSQC spectra acquired for H97N 10L-fCzrA in the absence of added Zn(II) (blue cross-peaks) and addition of 1.0 molar equiv of Zn(II) (green contours) and 2.0 molar equiv of Zn(II) (red cross-peaks). (A) Resonances outside of the primary metal binding site including E18 and L23 (α1), Leu34 (α2), and Leu68 (turn region between α5 and β1). (B) Resonances from the C-terminal α5 helix.

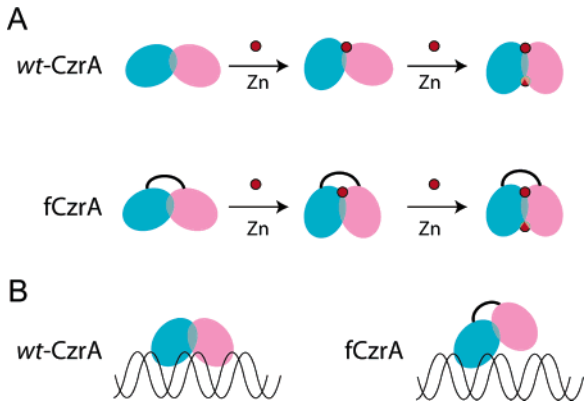

Figure 8. Cartoon representation illustrating the effect of a covalent linker on the structural and DNA-binding properties of CzrA. (A) Zn(II) binds to *wt*-CzrA in two discreet steps, the first of which introduces significant structural asymmetry into the dimer. Less structural asymmetry is introduced into 10L-fCzrA upon Zn(II) binding which is manifest as slightly positive cooperativity of Zn(II) binding. (B) The tether that connects 10L- and 5L-CzrA may be of insufficient length to allow both α4 reading heads access to successive major grooves in the operator-promoter region. Note that precise quaternary structural changes that accompany Zn(II) vs DNA binding are not yet known.

arranged on opposite sides of the DNA as previously shown for DtxR[40] and speculated for Fur-family metalloregulators.[8,41] Regardless of the true arrangement of homodimers, a simple modeling experiment reveals that the α1 helices must move out of the way (see Figure 1B) or the DNA must be underwound and/or strongly bent in order for the α4 (αR) helices, the "reading heads" of ArsR/SmtB family proteins, to insert into successive major grooves in the standard fashion.[42] One possibility therefore is that just one of the two protomer domains of 10L- and 5L-fCzrAs might make sequence-specific contacts with the DNA in the $fP_2{\cdot}D$ and $(fP_2)_2{\cdot}D$ complexes, due to a strongly hindered quaternary structural change that might have to occur upon DNA binding (see Figure 8B). In this case, ΔG_c might be expected to be half that of *wt*-CzrA, which is essentially what is observed for 10L- and 5L-fCzrAs (Table 2).

A single functional metal site in the homodimer drives significant allosteric regulation of DNA binding by fCzrAs. Since 5L-fCzrA binds a single metal ion with high affinity, yet is functional in allosteric regulation, this suggested the possibility that occupancy of just one α5 site might be sufficient to induce significant allosteric coupling. We tested this directly by inactivating one of the two sites independently via introduction of a single poorly metal ligating (H97N or H197N) substitution into metal sites 1 or 2, respectively. We show that occupancy of a single α5 metal site in 10L-fCzrA induces ~77% (69% from ΔG^1_c and 83% from ΔG^2_c) of the allosteric coupling free energy of the parent wild-type 10L-fCzrA (Table 2; Figure 6). This finding is incompatible with a concerted "all-or-none" model and, thus, reveals that the filling of just one of the α5 sites on the CzrO bound homodimer results in significant dissociation of the CzrA homodimer. This result is in accord with the HSQC spectra (Figure 7) which show that Zn(II) occupancy of the one remaining functional α5 site of H97N-10L-fCzrA results in significant quaternary structural switching; in particular, the hydrogen bonding pathway that originates with the $NH^{\epsilon 2}$ group of His197 and connects the metal site to the DNA binding helix of the opposite protomer domain is clearly established (Figure 7). Indeed, previous metal-induced SmtB–SmtO dissociation experiments reveal that while occupancy of both Zn(II) sites was necessary to effect full dissociation, substoichiometric Zn(II) concentrations were partially effective.[12] Finally, these properties of CzrA are largely in accord with recent studies of two additional ArsR/SmtB regulators, the Cd(II)/Pb(II)-sensor *M. tuberculosis* CmtR[43,44] and the Zn(II)/Cd(II)/Pb(II)-sensor *Anabaena* AztR.[45] In both cases, each regulator binds inducing metals with limiting stoichiometries of one per homodimer, i.e., strong negative cooperativity, which is likely sufficient to induce functional derepression in vivo.[43,45]

Summary

In this report, we outline a general strategy that exploits a series of covalently tethered "fused" dimers characterized by varying linker lengths to break the intrinsic 2-fold molecular symmetry within a homodimeric protein. This variable linker-

(39) Kar, S. R.; Lebowitz, J.; Blume, S.; Taylor, K. B.; Hall, L. M. *Biochemistry* **2001**, *40*, 13378−13389.
(40) White, A.; Ding, X.; vanderSpek, J. C.; Murphy, J. R.; Ringe, D. *Nature* **1998**, *394*, 502−506.
(41) Pohl, E.; Haller, J. C.; Mijovilovich, A.; Meyer-Klaucke, W.; Garman, E.; Vasil, M. L. *Mol. Microbiol.* **2003**, *47*, 903−915.
(42) Cook, W. J.; Kar, S. R.; Taylor, K. B.; Hall, L. M. *J. Mol. Biol.* **1998**, *275*, 337−346.
(43) Cavet, J. S.; Graham, A. I.; Meng, W.; Robinson, N. J. *J. Biol. Chem.* **2003**, *278*, 44560−44566.
(44) Wang, Y.; Hemmingsen, L.; Giedroc, D. P. *Biochemistry* **2005**, *44*, 8976−8988.
(45) Liu, T.; Golden, J. A.; Giedroc, D. P. *Biochemistry* **2005**, *44*, 8673−8683.

length approach is generally applicable to the study of oligomeric allosteric systems where the N- and C-termini are close enough to enable facile tethering and where quaternary structural changes form the basis of biological regulation, particularly in cases where high-resolution structural information on the various conformational states is lacking.

These studies lay the important groundwork for further use of the fCzrA system to site-specifically incorporate fluorescence resonance energy transfer (FRET) donor and acceptor pairs into individual protomer domains.[46] This will allow observation of the equilibrium distribution of the quaternary structural states accessible to fCzrA derivatives and, potentially, the Zn(II)-dependence of the kinetics of their interconversion.[27] More importantly, we show here that 10L- and 15L-fCzrAs may be amenable to the development of a picomolar yet tunable[37] zinc-sensing optical or bioelectronic device.[47] A necessary requirement is that the structure and metal binding affinity of the sensing sites in the fused dimer be unperturbed; this has been clearly established here at least for Zn(II). The affinity of the Zn(II) site is also readily tunable, via perturbation of first shell ligands[33] and perhaps the second shell[48] interactions as well; this would permit the development of a panel of fCzrAs characterized by a wide range of K_{Zn} which could be used to accurately determine free Zn(II) concentrations in situ. However, it is not yet known if the quaternary structural change in CzrA is large enough to permit its detection using traditional FRET methodologies. In this case, other approaches that might be amenable to detection of relatively smaller quaternary structural conformational changes, including one recently described based on CdSe nanoparticles,[25] are of high interest in this regard.

Experimental Section

Materials. Restriction endonucleases, DNA ligase, and DNA polymerase were from Stratagene and Invitrogen. Oligonucleotides were purchased from Integrated DNA Technologies (Coralville, IA). Ultrapure $CoCl_2$ and $ZnSO_4$ salts were obtained from Johnson Matthey (Raystan, U.K.), and solution concentrations were measured by using a Perkin-Elmer AAnalyst 700 atomic absorption spectrophotometer operating in flame mode.[32] Milli-Q deionized water was used for preparing all buffers and aqueous solutions.

Construction of Bacterial Expression Plasmids Encoding Single-Chain fCzrA Genes. A tandem array of two *czrA* genes was constructed by performing the steps outlined in Figure 1. The first *czrA* gene in the array (upstream gene) was created by PCR amplification using PCR primers A and B and pET3d-CzrA[11] as templates (see Figure 1). Primer A (5′-GTA ACC ATG GCA GAA CAA TAT TCA GAA ATA AAT AC-3′) introduces a *Nco*1 restriction site (underlined) overlapping the start codon for CzrA. Primer B simultaneously eliminates the stop codon of *czrA* and introduces a 15 or 30 nucleotide cassette, encoding for $(Ser_1Gly_4)_n$ (n = 1 or 2), respectively. The sequence of primer B for 5L-fCzrA (denoted B-5) construction was 5′-GTA TCT GTA TTT ATG GAA CCA CCA CCA CCT AAC CCA CTT TCT TTA GGA TGA TTC GCG TG-3′, and that for 10L-fCzrA (B-10) is 5′-GGA ACC ACC ACC ACC GGA ACC ACC ACC ACC TAA CCC ACT TTC TTT AG-3′. The second (downstream) *czrA* gene was amplified by PCR using the same template and primers B′ and C, with primer B′ complementary to primer B (for 5L-fCzrA, B′-5): 5′-GTA TCT GTA TTT ATG GAA CCA CCA CCA CCT AAC CCA CTT TCT TTA GGA TGA TTC GCG TG-3′ and 10L-fCzrA (B′10): 5′-GGT GGT GGT GGT TCC GGT GGT GGT GGT TCC ATA AAT ACA GAT ACA TTA G-3′) and primer C (5′-GCA GCC GGATCC ACT AGT AAC GGC C-3′) which contains a *Bam*H1 restriction site (underlined). Both the upstream and downstream genes were PCR-amplified in separate tubes, and product was purified with a PCR purification kit. Stepwise PCR was then carried out to fuse the upstream and downstream genes exploiting the complementary B and B′ primers that encode the linker segment in each case, to be used as a template for the second PCR step. Mixed PCR products were placed at 95 °C for 5 min and then cooled to 37 °C slowly in an oven to increase the population of the less stable DNA duplex hybridized at the B/B′ linker sequence only. Five "cycles" of PCR amplification was done, after which time, primers A and C were added in order to amplify the gene encoding fCzrA for an additional 30 PCR cycles. The resulting fragment encoding the tandem array of *czrA* genes was purified by agarose gel (1.8%) electrophoresis, restricted with *Bam*H1 and *Nco*1 and subcloned into *Bam*H1/*Nco*1-restricted pET3d to create pET-5L-fCzrA and pET-10L-fCzrA, respectively. The overexpression plasmid encoding 15L-fCzrA (pET-15L-fCzrA) was prepared by insertion of a 15-nucleotide cassette encoding a single Gly_4Ser_1 repeat into pET-10L-fCzrA using QuickChange mutagenesis with PCR primers D and D′ (D: 5′-GCG AAT CAT CCT AAA GAA AGT GGG TTA GGC GGC GGC GGC AGT GGT GGT GGT GGT TCC GGT GG-3′; D′: complementary sequence). Two other overexpression plasmids were also constructed that contained a single H97N substitution into either the upstream (pET-10L−H97N-wt-fCzrA) or downstream gene (pET-10L-wt-H97N-fCzrA) in the tandem gene array connected by the 10-aa linker. The same double PCR primer method was used for these constructions, except that, for pET-10L-H97N-wt-fCzrA, the primer A/B-10 pair was used on pET3d-H97N-CzrA as the first PCR template, and the primer B′-10/C pair, on pET3d-CzrA as the second template. Likewise, for pET-10L-wt-H97N-fCzrA, the primer B′-10/C pair was used with pET3d-H97N-CzrA as the template, and the A/B-10 amplification was carried out on pET3d-CzrA as above. An overexpressing clone for CzrA(Δ3−9) was obtained using QuickChange mutagenesis and pET3d-CzrA[11] as the template. Both strands of all overexpression plasmids were sequenced to confirm their integrity.

Protein Purification. Recombinant 5L-fCzrA, 10-L-fCzrA, and 15L-fCzrA were expressed from pET-5L-fCzrA, pET-10L-fCzrA, and pET-15L-fCzrA, respectively, in *Escherichia coli* BL21(DE3)/*pLysS* and were grown on 1.5% LB agar plates containing 0.1 mg/mL ampicillin at 37 °C. The growth, expression, and purification of fCzrAs were carried out by using the procedure described for SmtB,[32] except that DTT was excluded from the purification because CzrA does not have cysteine residues.[11] The final protein preparations were estimated to be ≥95% pure in overloaded SDS-PAGE gels with contaminating Zn(II) contents estimated to be ≤0.1 mol/mol by atomic absorption on a Perkin-Elmer AAnalyst 700 atomic absorption spectrophotometer.

Metal Binding Experiments. All metal binding experiments were carried out by using a Hewlett-Packard model 8452A spectrophotometer essentially as described. A zinc chelator indicator dye, Quin-2 (K_{Zn} = 2.7×10^{11} M^{-1} at pH 7.0 and 25 °C),[32] was employed to measure the Zn(II) binding constants for fused CzrAs exactly as previously described,[10] with a model that links two stepwise Zn(II) binding events to the dimer defined by K_{Zn1} and K_{Zn2} to the monomer−dimer equilibrium (in the case of *wt*-CzrA only) defined by K_{dimer} as measured previously.[11] Each data point was taken 30 min after each addition of $ZnSO_4$ to ensure that equilibrium was reached.

NMR Spectroscopy. Uniformly ^{15}N-labeled *wt*-CzrA, 10L-fCzrA, and H97N 10L-fCzrA were prepared as previously described.[10] $^1H-^{15}N$ HSQC spectra were acquired on a Varian Unity Inova 500 MHz spectrometer in the Biomolecular NMR Laboratory at Texas A&M University. The sample contained 0.1−0.2 mM CzrA dimer equivalents in 5 mM d_{18}-Mes and 100 mM NaCl (pH 6.0), 37 °C. Chemical shift referencing is relative to DSS.

(46) Slaughter, B. D.; Unruh, J. R.; Allen, M. W.; Bieber Urbauer, R. J.; Johnson, C. K. *Biochemistry* **2005**, *44*, 3694−3707.
(47) Zeng, H. H.; Thompson, R. B.; Maliwal, B. P.; Fones, G. R.; Moffett, J. W.; Fierke, C. A. *Anal. Chem.* **2003**, *75*, 6807−6812.
(48) Hunt, J. A.; Fierke, C. A. *J. Biol. Chem.* **1997**, *272*, 20364−20372.

Scheme 1

$$fP_2 + D \overset{K_1}{\rightleftarrows} fP_2{\cdot}D + fP_2 \overset{K_2}{\rightleftarrows} (fP_2)_2{\cdot}D + fP_2 \overset{K_3}{\rightleftarrows} (fP_2)_3{\cdot}D + fP_2 \overset{K_4}{\rightleftarrows} (fP_2)_4{\cdot}D$$

Scheme 2

$$P + P \overset{K_{dimer}}{\rightleftarrows} P_2 + D \overset{K_1}{\rightleftarrows} P_2{\cdot}D + P_2 \overset{K_2}{\rightleftarrows} (P_2)_2{\cdot}D + P_2 \overset{K_3}{\rightleftarrows} (P_2)_3{\cdot}D + P_2 \overset{K_4}{\rightleftarrows} (P_2)_4{\cdot}D$$

Equilibrium Urea Denaturation Experiments. The conformational stabilities, $\Delta G(H_2O)$, of apo *wt*-CzrA, 5L-fCzrA, 10L-fCzrA, and 15L-fCzrA were determined using urea denaturation as monitored by circular dichroism spectroscopy with an Aviv 62DS spectropolarimeter. Stock solutions of urea were prepared fresh daily. Protein stock solutions were prepared in 10 mM sodium phosphate, 0.1 M NaCl at pH 7.0. Urea concentrations were determined by refractive index.[49] The unfolding curves were fit to a two-state unfolding model using an equation derived from the linear extrapolation method (LEM).[50−52]

$$[\Theta]_{obsd} = \{([\Theta_N] + a_N[D]) + ([\Theta_D] + a_D[D]) \times \exp[m([D] - C_m)/RT]\}/\{1 + \exp[m([D] - C_m)/RT]\}$$

where $[\Theta]_{obsd}$ is the molar ellipticity measured at each molar denaturant concentration, [D], and a_N and a_D are the denaturant-dependent slopes and $[\Theta_N]$ and $[\Theta_D]$ are the *y*-intercepts of the pre- and post-transition baselines, respectively. The parameter *m* is a measure of the dependence of the ΔG on [D], and C_m is the midpoint of the denaturation curve, in this case, $[urea]_{1/2}$. $\Delta G(H_2O)$ is obtained by multiplying the C_m and *m* values.

DNA Binding Experiments. Fluorescence anisotropy experiments were carried out with an ISS PC1 photon counting spectrofluorometer with both fluorescein-labeled 57-bp and Cy3-labeled 41-bp CzrO-containing oligonucleotides, with the data acquired and analyzed as previously described.[11] The DNA concentration in all cases was fixed at 4.0 nM in 10 mM Hepes, 0.4 M NaCl, pH 7.0. The DNA binding isotherms were fit using DYNAFIT[53] to a sequential binding model of up to 4 mol of fCzrA (fP_2) per mol of DNA duplex (D) (Scheme 1), exactly as described previously for homodimeric CzrA (Scheme 2), except that the monomer−dimer equilibrium is obviously not present.[11]

The characteristic anisotropies, r_i, for each protein−DNA complex were estimated from a binding isotherm obtained upon titration of 0.8 to 1.0 μM dsDNA with *wt*-CzrA and 15L-fCzrA (i.e., stoichiometric binding conditions). They were determined to be $r_D = 0.113$ for free DNA; $r_{fP2\cdot D} = 0.127$, $r_{(fP2)2\cdot D} = 0.141$, $r_{(fP2)3\cdot D} = 0.155$, $r_{(fP2)4\cdot D} = 0.169$ for CzrA-fluorescein-labeled 57-bp DNA complexes; and $r_D = 0.293$, $r_{fP2\cdot D} = 0.307$, $r_{(fP2)2\cdot D} = 0.321$, $r_{(fP2)3\cdot D} = 0.335$ for CzrA-Cy3-labeled 41-bp DNA complexes. These characteristic anisotropy values were used as fixed parameters in the nonlinear least-squares fits to obtain best-fit values for each stepwise K_i (see Schemes 1 and 2).[4]

Acknowledgment. We thank Dr. Mario Pennella for comments on the manuscript and the gift of *wt*-CzrA and Maria Shubina for help in purifying fused CzrAs. We also gratefully acknowledge Drs. A. Razvi and J. M. Scholtz for help in acquiring the urea denaturation curves. This work was supported by grants from the NIH (GM042569), Robert A Welch Foundation (A-1295), and TAMU Life Sciences Task Force Program of Excellence (POE-06).

Supporting Information Available: The physical characterization of CzrA(Δ3−9), urea denaturation experiments, and complete $^1H-^{15}N$ HSQC spectra of *wt*-CzrA, 10L-fCzrA, and H97N 10L-fCzrA are available. This material is available free of charge via the Internet at http://pubs.acs.org.

JA0546828

(49) Pace, C. N. *Methods Enzymol.* **1986**, *131*, 266−280.
(50) Pace, C. N.; Scholtz, J. M. *Protein Structure: A Practical Approach*; IRL Press: Oxford, 1997; pp 229−321.
(51) Nicholson, E. M.; Scholtz, J. M. *Biochemistry* **1996**, *35*, 11369−11378.
(52) Santoro, M. M.; Bolen, D. W. *Biochemistry* **1988**, *27*, 8063−8068.
(53) Kuzmic, P. *Anal. Biochem.* **1996**, *237*, 260−273.
(54) Koradi, R.; Billeter, M.; Wuthrich, K. *J. Mol. Graph.* **1996**, *14*, *51−55*, 29−32.